MOLECULAR METABOLISM

Insulin resistance *per se* drives early and reversible dysbiosis-mediated gut barrier impairment and bactericidal dysfunction

Dalale Gueddouri [1], Michèle Caüzac [1], Véronique Fauveau [1], Fadila Benhamed [1], Wafa Charifi [1], Lucie Beaudoin [1], Matthieu Rouland [1], Florian Sicherre [1], Agnès Lehuen [1], Catherine Postic [1], Gaëlle Boudry [2], Anne-Françoise Burnol [1,3], Sandra Guilmeau [1,*,3]

ABSTRACT

Objective: A common feature of metabolic diseases is their association with chronic low-grade inflammation. While enhanced gut permeability and systemic bacterial endotoxin translocation have been suggested as key players of this metaflammation, the mechanistic bases underlying these features upon the diabesity cascade remain partly understood.

Methods: Here, we show in mice that, independently of obesity, the induction of acute and global insulin resistance and associated hyperglycemia, upon treatment with an insulin receptor (IR) antagonist (S961), elicits gut hyperpermeability without triggering systemic inflammatory response.

Results: Of note, S961-treated diabetic mice display major defects of gut barrier epithelial functions, such as increased epithelial paracellular permeability and impaired cell-cell junction integrity. We also observed in these mice the early onset of a severe gut dysbiosis, as characterized by the bloom of pro-inflammatory Proteobacteria, and the later collapse of Paneth cells antimicrobial defense. Interestingly, S961 treatment discontinuation is sufficient to promptly restore both the gut microbial balance and the intestinal barrier integrity. Moreover, fecal transplant approaches further confirm that S961-mediated dybiosis contributes at least partly to the disruption of the gut selective epithelial permeability upon diabetic states.

Conclusions: Together, our results highlight that insulin signaling is an indispensable gatekeeper of intestinal barrier integrity, acting as a safeguard against microbial imbalance and acute infections by enteropathogens.

1. INTRODUCTION

One of the hallmarks of obesity and associated type 2 diabetes (T2D) is the occurrence of a chronic low-grade inflammation [1—5]. While this subclinical inflammatory state has long been considered to pave the way for insulin resistance, the mechanistic bases for this metaflammation remain partially understood. Compelling evidence has now linked the enhanced systemic inflammatory tone that is observed upon obesity with adipocyte hypertrophy and associated dysregulated adipokine secretion profile, as well as macrophage infiltration into adipose tissue [6—8]. However, more recent investigations have also brought to light some intestinal dysfunctions, such as enhanced gut permeability and dysbacteriosis-mediated endotoxemia, as potential key players in this feature [9].

The gastrointestinal tract is a specialized organ, which nurtures dynamic interactions with a highly complex environment in order to maintain a homeostatic steady state. Under healthy conditions, the luminal gut microbiota ensures vital roles, such as digestion, development of host immune system, and defense against pathogens, but concomitantly represents a threat of infection. Therefore, intestinal cells collectively ensure, through a two-layer organization, a selective barrier function, by allowing an efficient transcellular transport of nutrients, while rigorously preventing the flow of immune-stimulatory bacterial products across the epithelium. Achieved by epithelial cells, the physical barrier surface shapes the microbiota composition and prevents bacterial adhesion partly through the bactericidal activity of Paneth cells and the production of mucus by goblet cells. In parallel, it also regulates the paracellular diffusion to the host tissues through cell—cell junctional complexes. Beneath the intestinal epithelium, the deep functional barrier that involves immune cell populations of the *lamina propria* discriminates between indigenous microorganisms and enteropathogens and coordinates an adapted immune response [10]. While disruption of gut barrier integrity enables opportunistic bacterial endotoxin translocation into the vasculature, the importance of impaired intestinal permeability in the pathogenesis of obesity-related metabolic alterations and T2D was first demonstrated by the

pioneering study of Cani et al. [11]. Indeed, by mimicking the enhanced trans-epithelial permeability and systemic influx of Gram-negative bacteria-derived lipopolysaccharide (LPS) that are observed upon high-fat diet-induced obesity, as well as in obesity and T2D mice models (*db/db*) [12,13], metabolic endotoxemia was identified as a key contributing factor in the initiation of dysregulated inflammatory tone, body weight gain, and diabetes onset. Moreover, reduced endotoxemia and metabolic improvement following antibiotic treatment of both high-fat diet-fed and *ob/ob* mice further suggested that gut dysbiosis induced by obesity could be a primary defect involved in the onset of gut hyperpermeability [11,14]. A lower phylogenetic diversity with a loss of commensal bacteria and a bloom of pathobionts was indeed reported upon obese conditions [15,16].

While most studies have focused on the emergence of gut dysbiosis and its deleterious intestinal outcomes upon obesity and associated diabetic conditions, induction of insulinopenia by treatment of lean mice with streptozotocin (STZ) was also reported to trigger intestinal microbial imbalance and alterations of various intestinal barrier components [17—19], indicating that blunted insulin action and concomitant hyperglycemia might be at play independently of adiposity. Interestingly, rather than obesity, hemoglobin A1c (HbA1c), indicative of an individual's three-month average plasma glucose concentration, was also associated with the systemic influx of microbial products in humans [17]. At the mechanistic level, STZ-induced hyperglycemic states *per se* were proposed to contribute to enhanced gut permeability, through glucose metabolism and transcriptional reprogramming in intestinal epithelial cells, independently of the onset of dysbiosis [17]. However, STZ intracellular uptake by GLUT2 [20], the expression of which in enterocytes is enhanced by STZ treatment [21,22], as well as STZ potency to act as an antibiotic against gram-negative bacteria [23], suggest that this diabetic model may have important limitations when investigating intestinal outcomes, as STZ could directly alter both epithelial cells functions and gut microbiota composition.

Therefore, in order to kinetically identify the consequences of insulin sensitivity changes on gut barrier integrity in the absence of obesity, we used a lean mouse model of reversible insulin resistance. The infusion of S961, a selective antagonist of the insulin receptor (IR), which rapidly induced systemic insulin resistance concomitantly to hyperglycemia and hyperinsulinemia, resulted in gut hyperpermeability associated with a modest local inflammation, and discontinuation of the treatment with S961 was sufficient to promptly and totally reverse this phenotype. At the mechanistic level, our study revealed that among the various components of the gut barrier, the major alterations were the early onset of a severe gut dysbiosis, as characterized by the bloom of pro-inflammatory Proteobacteria, and the later collapse of Paneth cells antimicrobial defense. Of note, fecal transplantation approaches further revealed that such S961-mediated microbial imbalance contributes at least partly to the outbreak of enhanced gut permeability upon hyperglycemic conditions. In conclusion, the present study demonstrates that, independently of obesity, global insulin resistance plays a critical role in reshaping a deleterious gut microbiota, thereby impairing epithelial integrity, which could contribute to the increased risk of the chronic inflammatory response observed in metabolic diseases.

2. MATERIAL AND METHODS

Animals and treatments. All procedures were carried out according to the French guidelines for the care and use of experimental animals and were approved by the "Direction départementale des services vétérinaires de Paris". ALZET® mini osmotic pumps were implanted subcutaneously in eight-week-old male C57Bl/6 J mice to infuse either S961,

an insulin receptor (IR) peptide antagonist (Novo Nordisk) (20 nmol/week), or PBS, as vehicle control, at 0.5 µl/h for 1 week as previously described [24] (PBS and S961 groups). In order to reverse the blockade of insulin signaling, pumps were removed after 7 days of treatment, and mice were studied 7 days after removal of the pumps (groups revPBS and revS961). The various experimental groups were housed in separate cages. Stools were collected and stored at −80 °C for subsequent analyses. For IR downstream signaling analyses, insulin (5 UI/kg) was injected *i.p.* following a 4 h fast, and mice were sacrificed after 10 min. Tissue samples were immediately dissected, frozen in liquid nitrogen, and stored at −80° until further analyses. The intestinal segments were flushed with cold PBS, longitudinally opened, and the gut mucosa was scratched using a glass slide before snap freezing.

Insulin tolerance tests. Insulin tolerance tests (0.75 units/kg body weight, *i.p.*) were performed in unrestrained conscious male mice after a 4-h fast, and blood glucose was measured using an Accu-Check glucometer (Roche Diabetes Care).

Cell preparations. IEC were prepared from the upper (USI, corresponding to duodenum and jejunum) and lower (LSI, corresponding to ileum) small intestine, and the colon. Gut segments were incubated in chelating solution (15 mM EDTA, 1 mM DTT in PBS) for 30 min at 37 °C under shaking at 100 rpm. Isolated cells were pelleted, snap-frozen in liquid nitrogen, and stored at −80 °C until further protein and gene expression analyses. For isolation of *lamina propria* cells, mice were sacrificed and the ileum was removed from the mice, cleared from feces, fat tissue, and Peyer's patches using HBSS without Ca^{2+} and Mg^{2+} containing 10 mM HEPES solution. Miltenyi Lamina Propria Dissociation Kit for mouse was used to prepare epithelial and *lamina propria* cells. After passage through a 100 µm filter, the cell suspension was subjected to Percoll (GE Healthcare) density gradient of 40% and 80%, and the interface between the layers containing intraepithelial lymphocytes or *lamina propria* lymphocytes were collected. Fractions were then either suspended in PBS containing 2% FCS and 0.1% sodium azide before further FACS analyses, or snap-frozen for further RT-qPCR investigations.

Western blot analyses. IECs or gut mucosa scrapping were solubilized at 4 °C in a lysis buffer 'Tris-HCl 50 mM, NaCl 150 mM, EDTA 5 mM, Triton X-100 1%) containing protease inhibitor (2x) (Complete tablet Easy pack, Roche) and phosphatases inhibitors (NaF 10 mM, Na_3VO_4 4 mM, $Na_4P_2O_7$ 60 mM). Supernatants were collected after a 15-min centrifugation at 13,000 rpm at 4 °C. Proteins were quantified using the Bradford method (BioRad Protein Assay). The protein extracts were then subjected to SDS-PAGE electrophoresis and immunoblotted with the following primary antibodies: anti-pAkt (Ser473) (CST#4060), anti-Akt (CST#9272), anti-BiP (CST#3183), anti-CHOP (CST#5554), anti-NQO1 (CST#3187, Cell Signaling Technology), anti-p62 (PW9860, Enzo BML), or anti-GAPDH (sc-25778, Santa Cruz Biotechnologies). The immunoreactive bands were revealed using the Clarity Western ECL Substrate (BIO-RAD) Chemiluminescence, and analysis was performed with the ChemiDOc MP Imaging System (BIO-RAD).

RNA extraction and RT-qPCR analyses. Total RNAs were extracted from IECs using TRIzol® reagent (Life Technologies) according the manufacturer's protocol, and 1 µg was used for reverse transcription (Life Technologies). cDNAs were amplified by qPCR (LightCycler® 480 SYBR Green I Master, Roche) using the primers described in the Supplementary Table 1. mRNA levels were normalized over the expression of *GAPDH* and *TBP*.

Intestinal permeability. Overnight fasted mice were submitted to an oral gavage of FITC-dextran 4 kDa (FD4, 0.6 mg/g body weight) (TdB Consultancy) and 0.5% carboxymethycellulose solution including 6% Carmine red (Sigma) in order to evaluate gut transepithelial permeability normalized to intestinal transit. One hour after FD4 gavage,

peripheral blood was collected, and serum FITC-dextran concentrations were determined using a fluorescence spectrophotometer (Ex/Em 490/520 nm). The total intestinal transit time was measured by determination of the time between ingestion of carmine red and first appearance of the dye in feces.

Histological analyses and histopathological scoring. Gut samples from the proximal ileum and colon were fixed in 4% PFA, embedded in paraffin, and cut into 5 μm sections. After deparaffinization and rehydration, intestinal and colonic sections were stained using standard protocols with either hematoxylin-eosin (HE) or Alcian blue staining to evaluate mucus production. For Paneth cells immunolabelling, an anti-Lysozyme (Dako, EC.3.2.1.17, 1:200) primary antibody was used. Histopathological scoring was performed by blinded clinical evaluation using the following parameters [1]: severity of inflammation [2], ulceration depth [3], area involved in the ulcerative process [4], edema [5], vascular dilation, and [6] ischemia, and parameter values were used to generate a « total histological score ».

Flow cytometry. Ileal cells from the *lamina propria* were isolated using Lamina Propria Dissociation Kit (Miltenyi, 130-097-410) as previously described [25]. Each subset of *lamina propria* cells was analyzed *via* flow cytometry after 20 min of staining at 4 °C in PBS containing 2% fetal bovine serum and 0.1% sodium azide with the following antibodies: CD45 (APC-Cy7, 30F11); CD64 (BV605, X54−57.1); Ly-6C (BV510, HK1.4); Ly-6G (PE, 1A8); CD11b (BV785, M1/70); CD11c (APC, N418); CD103 (BV421, M290); CX3CR1 (PE-CF594, SA011F11); F4/80 (PE-Cy7, BM8); MHC Class II (AF700, M5/114-5-2). Data acquisition was processed using Biosciences LSR Fortessa (BD Biosciences). Gating and calculation of cell population frequencies were computed with FlowJo (Tree Star) analysis software. Macrophages were identified as CD45$^+$ CD19$^-$ TCRγδ$^-$ TCRβ$^-$ CD11b$^+$ cells, DCs were identified as CD45$^+$ CD19$^-$ TCRγδ$^-$ TCRβ$^-$ CD11b$^-$ CD206$^-$ CD11c$^+$ cells, T cells were identified as CD45$^+$ CD19$^-$ TCRβ$^+$ cells, and B cells were identified as CD45$^+$ TCRβ$^-$ CD19$^+$ cells. Gating strategies to determine macrophages, DC, T, and B cells are presented in Fig S1.

Transmission electron microscopy. Samples from LSI were analyzed under a JEOL 1011 transmission electron microscope with a GATAN Erlangshen CCD (charge-coupled device) camera. Acquisitions were processed using software « Digital Micrograph » and ImageJ.

Microbiota analysis. Bacterial DNA was extracted from luminal content samples using the ZR fecal DNA Miniprep kit (Zymo Research, USA). The V3−V4 region of 16S rDNA was amplified using the following primers: CTTTCCCTACACGACGCTCTTCCGATCTCTACTCCTACGGGAGGCAGCAG (V3F) and GGAGTTCAGACGTGTGCTCTTCCGATCT TACCAGGGTATCTAATCC (V4R), Taq Phusion (New England Biolabs), and dNTP (New England Biolabs) during 25 cycles (10 s at 98 °C, 30s at 45 °C, 45s at 72 °C). Purity of amplicons was checked on agarose gels before sequencing using Illumina Miseq technology, performed at the Genotoul Get-Plage facility (Toulouse, France). Raw sequences were analyzed using the bioinformatic pipeline FROGS [26]. Briefly, quality control was performed using Cutadapt (version 1.18) and Flash (version 1.2.11) to delete sequences not between 380 and 500 bp, sequences with ambiguous bases, and sequences that do not contain good primers. Clustering was then performed using Swarm v2.1.2 with an aggregation maximal distance of 3 bases. Chimera were removed using VSEARCH (v2.9.1) with cross-sample validation. PhiX contamination was removed using VSEARCH. Affiliation was performed using the silva 123 16S database and NCBI Blastn++. A phylogenetic tree was constructed using FastTree (v2.1.10), and sample depth was normalized using GMPR. Physloseq package was used for biostatistical process. The number of observed species and Shannon index (evenness of the species

abundance distribution) were calculated to estimate alpha-diversity. Beta-diversity was evaluated by calculating Jaccard distances between samples. Ordination using principal coordinates analyses was performed to represent samples on a 2D plot. Relative abundances of the 5 major phyla were compared using ANOVA.

Fecal Microbiota Transplantation. Eight-week-old male C57Bl/6 mice infused with PBS or S961 were used as fecal microbiota donors. These mice were acclimated in the facility during 1 week before the beginning of the experiment. Feces from donor mice were collected in sterile containers (GENbox anaer, Biomerieux) and immediately diluted (1:20 w/vol) in sterile PBS prepared with 0.5 g/l cystein. Colonization was achieved by daily intragastric gavage with 200 μl of inoculum for three consecutive days in 3-week-old specific-pathogen-free (SPF) male C57Bl/6 J recipient mice, as previously described [27].

Biochemical analyses. Fecal lysozyme activity (EnzChek lysozyme assay kit, Molecular Probes), as well as fecal lipocaline-2 (Mouse Lipocalin-2/NGA Duo set ELISA kit, R&Systems) and albumin (mouse albumin ELISA kit, Bethyl Labs) contents, were measured using the indicated commercial assays according to the manufacturers' instructions. Plasma LBP (mouse LBP ELISA kit, Abcam) and insulin (mouse ultrasensible insulin ELISA, ALPCO) concentrations and gut MPO contents (Mouse MPO ELISA kit, HycultBiotech) were quantified using the indicated ELISA assays.

Statistical analyses. All values are presented as means ± SEM. Statistical analyses were performed with Prism software (Graph Pad V.8.3). Datasets were compared using non-parametric two-tailed Mann−Whitney U-test or analysis of variance (ANOVA) followed by Bonferroni post-test multiple comparisons. Statistical significance was assumed at P values < 0.05.

3. RESULTS

3.1. S961-associated insulin resistance compromises gut barrier integrity in lean mice

In order to determine the impact of blunted insulin signaling on gut barrier integrity independently of obesity, we developed a mouse model of inducible and reversible systemic insulin resistance. To that end, osmotic pumps delivering the IR antagonist S961, or PBS as control, were implanted subcutaneously for 7 days in C57Bl/6 J mice (S961 and PBS mice, respectively). The reversibility of S961-induced defects was in turn evaluated in S961 and PBS mice that were allowed a 7-day recovery time frame after removal of the pumps (revS961 and revPBS mice, respectively). As illustrated in Figure 1A, treatment with S961 was accompanied by a significant weight loss, which was totally rescued 1−2 days following pump removal. Of note, S961 infusion promptly triggered a sustained hyperglycemia, and cessation of the S961 treatment allowed a rapid drop in blood glucose concentrations that reached control levels within 3 days (Figure 1B). Accordingly, serum insulin concentrations were markedly enhanced in S961-treated mice and returned to control values in revS961 mice (Figure 1C), thereby reflecting impaired hepatic insulin clearance in the absence of functional IR [28]. Insulin tolerance tests (ITT) indicated the onset of a severe insulin resistance upon 7 days infusion with S961 (Figure 1D), whereas insulin sensitivity was fully restored and even improved 7 days following cessation of the treatment (Figure 1E). This was further illustrated by a lower glycemia in revS961 mice when compared to the revPBS control group at 60 min after i.p insulin challenge (Figure 1E). In line with these results, examination of IR downstream signaling in major insulin target tissues, such as liver and skeletal muscle, indicated that insulin-induced Akt phosphorylation was reduced upon S961 treatment and totally rescued in revS961 mice
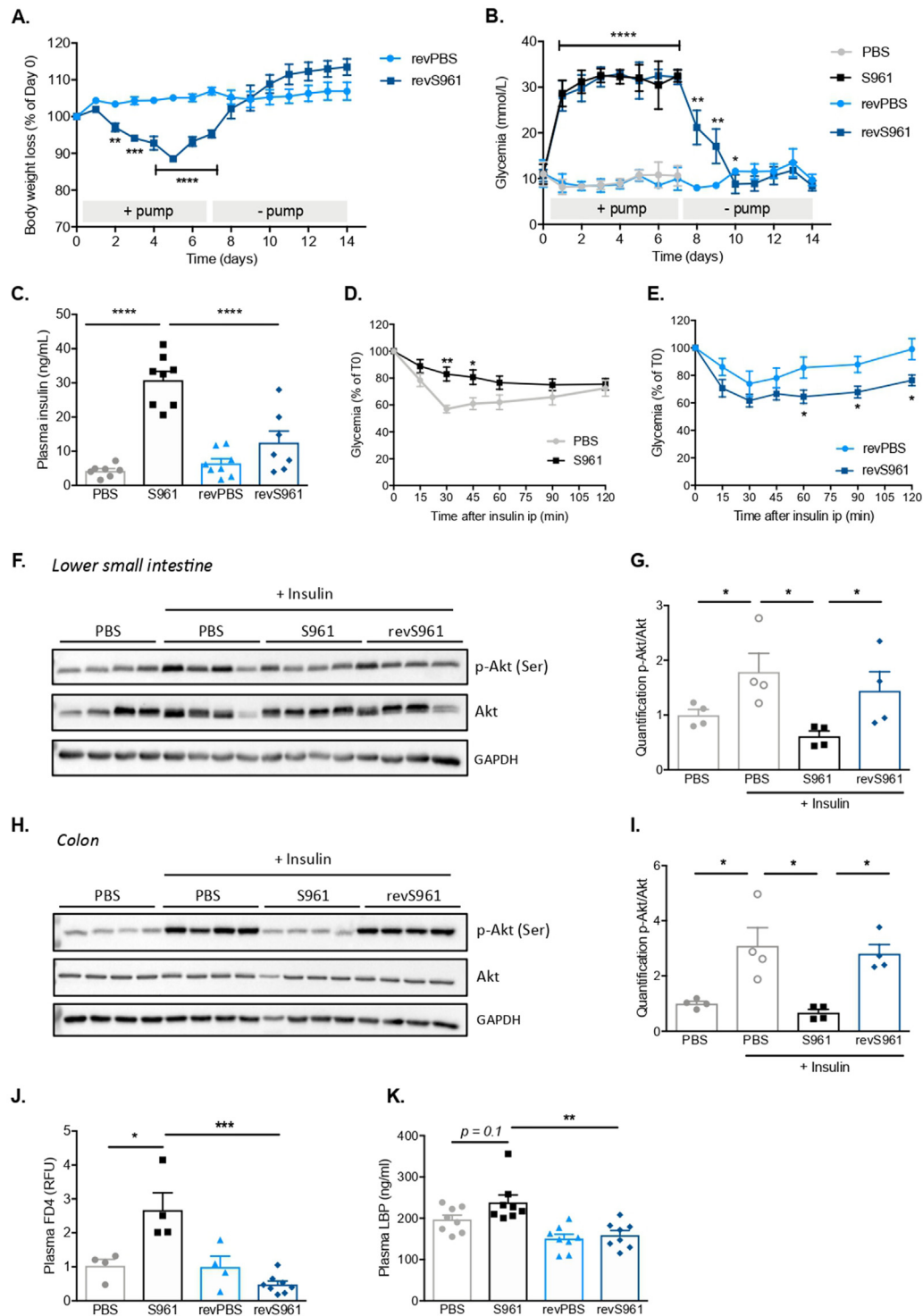
Figure 1: S961 induces global and reversible insulin resistance and enhances gut permeability in mice. (A) Kinetic of body weight loss and (B) post-prandial glycaemia in mice treated with PBS or S961 (20 nmol/wk) for 7 days (PBS, S961) through osmotic pump-mediated subcutaneous delivery (n = 8—16), or in mice studied during 7 days after pump removal (revPBS, revS961) (n = 4—8). (C) Portal insulin concentrations in 7-day PBS-or S961-treated mice that were fasted 4 h before refeeding overnight with 20% glucose (n = 7—8). (D) Insulin tolerance tests performed in PBS and S961 mice after 7 days of treatment (n = 12—16), or (E) in revPBS and revS961 mice one week after pump removal (n = 8—11). (F—I) Western blot analyses and relative quantifications of Akt activation (P-Akt levels normalized to total Akt) in ileal (F, G) and colonic epithelial cells (H, I) in mice submitted *in vivo* to an i.p. pulse of insulin (5UI/kg) for 10 min (n = 4). P-Akt and total Akt levels were first normalized to GAPDH on each corresponding blot (only GAPDH levels relative to total Akt blot are shown in F and H), and quantification of P-Akt/Akt levels (G, I) corresponds to the ratio of relative P-Akt/GAPDH levels on relative total Akt/GAPDH levels. (J) Intestinal permeability to FITC-dextran (FD4) (n = 4—8) and (K) plasma LBP concentrations (n = 8) in PBS and S961 mice after 7 days of treatment, or in revPBS and revS961 mice one week after pump removal. (A—E, G, I—K) Values are means ± SEM. *p < 0.05, **p < 0.01, ***p < 0.001, ****p < 0.0001 by ANOVA (B—C, G, I—K) or Mann—Whitney U-test (A, D-E).

following acute insulin pulse *in vivo* (Fig S2A—D). Of interest, S961 infusion similarly resulted in a striking reduction of insulin-driven Akt phosphorylation in epithelial cells from the ileum and the colon, while discontinuation of the treatment with S961 fully restored mucosal insulin signaling (Figure 1F—I).

While these data validated the reversible loss of downstream insulin signaling subsequent to transient S961 treatment, and further provided evidence that gut epithelium is an insulin sensitive organ, we next investigated the functional consequences of global insulin resistance *per se* (independently of obesity) on gut barrier integrity. *In vivo* gut permeability upon S961 treatment was evaluated through the measurement of FITC-dextran (FD4) transepithelial flux. One hour after oral gavage, plasma concentration of the FD4 tracer was significantly increased (2.7-fold) in S961-diabetic mice compared to PBS-treated mice (Figure 1J). Moreover, serum levels of LPS-binding protein (LBP), a surrogate marker of endotoxemia [11], was slightly, although not significantly, enhanced by S961 treatment (Figure 1K). Interestingly, similar values for both of these readouts of gut leakage were obtained in revS961 and control revPBS mice (Figure 1J—K), suggesting that the deleterious effects of insulin resistance and concomitant hyperglycemia on gut barrier function were reversible.

3.2. S961 treatment destabilizes epithelial cell junctions and promotes local inflammation

Since intercellular junctional complexes are critical components of epithelial integrity [29], we next performed histological as well as ultrastructural analyses of the gut epithelium from S961 and PBS-treated mice in order to explore the underlying mechanisms of S961-associated gut hyperpermeability. Of note, treatment with S961 did not cause any apparent histological defect in the ileum or in the colon, as shown on Fig S3A. However, a closer examination of the ileum through transmission electron microscopy (TEM) indicated that while tight and adherens junctions were classically observed in apical cell—cell contact regions of PBS mice, the epithelium of S961-diabetic mice appeared dramatically disorganized (Figure 2A). Notably, this was illustrated by the occurrence of cytosolic protrusions in the vicinity of intercellular spaces and brush border membranes, indicating loss of integrity of the epithelial cell monolayer (Figure 2A). In the colonic epithelium, cell—cell junctions were also disrupted following S961 treatment, as shown by enhanced spaces between adjacent cells and overflowing cytosolic contents at the apical membrane (Figure 2A). In accordance with these structural defects, the mRNA levels of genes encoding tight junction proteins (*CLDN4, OCL, ZO1*) were significantly decreased in ileal epithelial cells from mice treated with S961 for 7 days (Figure 2B), while only minor changes were observed at earlier time point (Fig S3B) or in the colonic epithelium of S961 mice, as compared to PBS-treated mice (Figure 2C).

We further examined whether those alterations of epithelial gut integrity upon S961-induced insulin resistance were associated with the onset of a low-grade inflammation. Despite the fact that S961 treatment triggered the disruption of gut mucosal barrier (Figure 1J—K) and the consecutive raise of capillary permeability, as documented by the 2.5-fold increase in albumin (66.5 kDa) released from blood vessels into the intestinal lumen (Figure 2D), this was not associated with systemic inflammation (Fig S3C). However, such a diabetic condition instead induced the onset of a slight intestinal inflammation, as shown by a 3-fold increase in lipocalin 2 fecal content and parallel unchanged neutrophil MPO activity (Figure 2E—F). Deeper evaluation of the cellular mechanisms underlying this local inflammatory state was performed by FACS analysis of immune cells populations isolated from the intestinal *lamina propria* of S961-treated mice. As compared to the PBS control group, S961-treated mice displayed an increased abundance of gut fully mature macrophages (CD11b$^+$ CD206$^+$) without changes in total CD11b$^+$ macrophages (Figure 2G—H), dendritic cells, or in B and T lymphocytes relative number (Fig S3D—F), suggesting some alterations in gut innate immunity upon blockade of insulin signaling. Of note, among cytokines involved in IL-22-mediated barrier function and host defense, which were previously implicated in the susceptibility of obese and diabetic mice to infection [17,30], only *IL2*3 mRNA levels were significantly increased by 3.7-fold in the intestinal *lamina propria* upon S961 challenge (Figure 2I). Together, these data indicate that the destabilization of intestinal epithelial cell junctions upon an acute S961-mediated insulin-resistant state only results in modest local inflammatory response.

3.3. Antibacterial activity of paneth cells is drastically impaired in S961-diabetic mice

By preventing bacterial adhesion and shaping the microbiome composition, mucus production by goblet cells and bactericidal activity of Paneth cells represent major players in gut barrier maintenance [10]. Therefore, we next performed a kinetic study to explore whether these epithelial features could underlie increased gut permeability and related local inflammatory response in S961-diabetic mice treated for 3 or 7 days. A progressive reduction of ileal mRNA levels encoding specific goblet cell markers (*Muc2, Tff3, Gob5*) was indeed observed following treatment with S961 (Figure 3A, S3A), while only minor significant changes were detected in the colon after 7 days of S961 infusion (Figure 3B), as compared to the PBS control group. Of note, parallel mucus staining with Alcian blue did not reveal any apparent modification in either the ileum or the colon during the S961-induced insulin resistant state, when compared to PBS-treated mice (Figure 3C).

Strikingly, quantification of Paneth cells markers, such as genes encoding antimicrobial peptides (*Defa3, Defcr5, Defa6, Ang4, Lyz*), demonstrated that their expression was consistently reduced by at least 50% in the ileum of 7-day S961-treated mice (Figure 3D), while no significant alterations could be detected at earlier time point (Fig S4B). Supporting a drastic deterioration of bactericidal defense by Paneth cells upon S961-induced diabetic conditions, ileal lysozyme immunolabelling was significantly diminished in S961-treated mice when compared to the PBS control group (Figure 3E). Ultrastructural analyses by TEM further revealed that S961 infusion triggered profound alterations to the Paneth cells morphology (Figure 3F). This was illustrated by the presence of large cytosolic vacuoles with clear and filamentous contents, and by the reduction of secretory granules' mean area and frequency in parallel with the appearance of abnormal thick and clear halos surrounding them (Figure 3F—H), consistent with the reduced fecal lysozyme content observed upon S961 treatment (Figure 3I). While Paneth cells have been reported as highly prone to abnormalities upon altered unfolded protein response [31], swollen and distended endoplasmic reticulum (ER) cisterns in Paneth cells from S961-receiving mice were reminiscent of ER stress (Figure 3F). Western blot analyses of ER stress markers on ileal epithelial cells further revealed a trend towards enhanced CHOP protein levels in diabetic S961 mice when compared to the control PBS group, while BiP expression was comparable between the two groups (Fig S5). Of note, a significant decrease of NQO1 expression in ileal epithelial cells following S961 treatment suggested that intestinal ER-associated oxidative stress defense was impaired upon diabetic conditions.
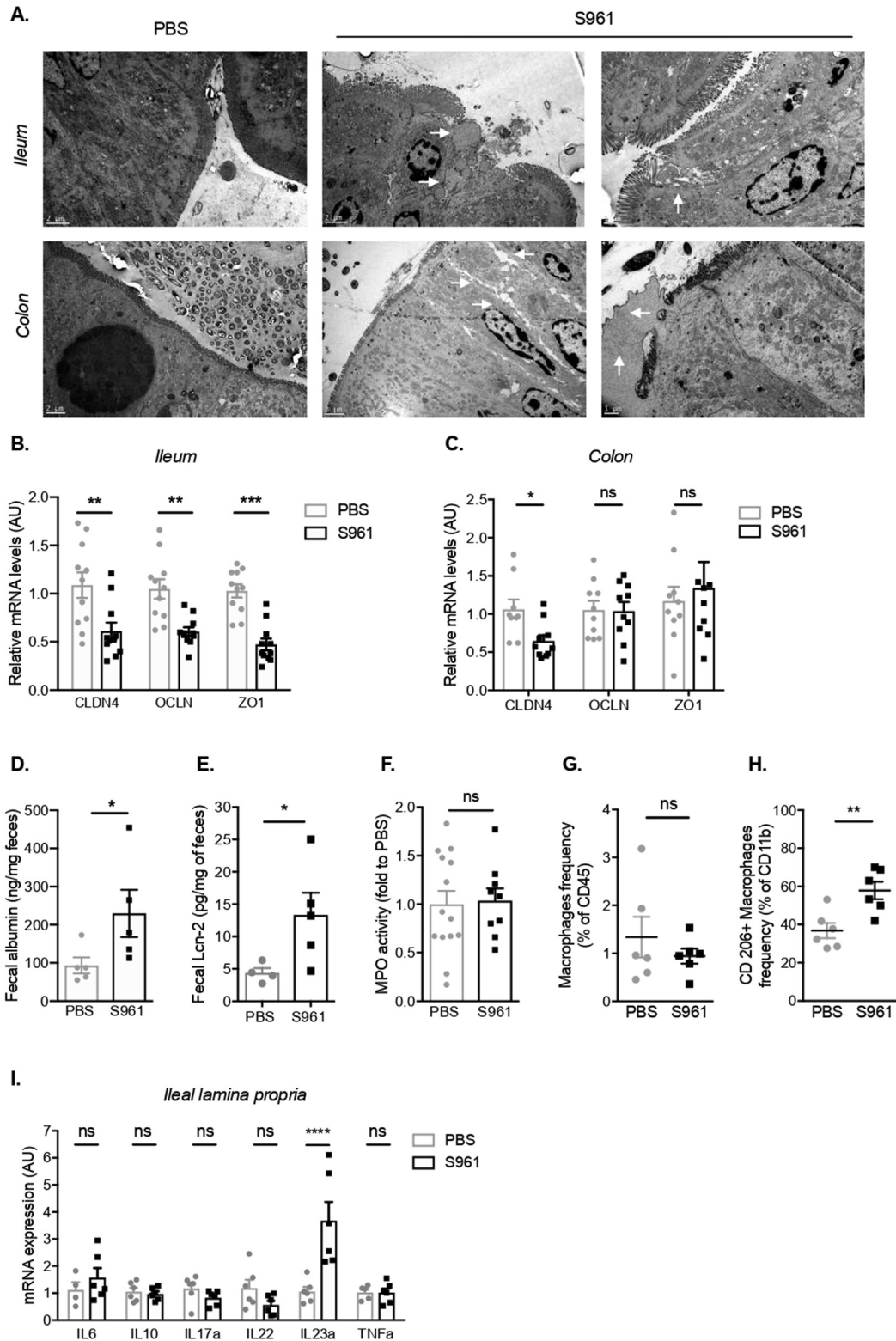
Figure 2: S961 treatment triggers gut barrier defects and low-grade intestinal inflammation. (A) Representative electron microscopy of ileal and colonic samples from PBS- and S961-treated mice after 7 days of treatment. Scale bars: 2 μm (left panels: PBS, S961), 1 μm (right panels). White arrows indicate ultrastructural abnormalities. (B, C) Relative mRNA levels (normalized to *Gapdh*) of tight junction markers in isolated epithelial cells from the ileum (B) and the colon (C) of indicated groups of mice (n = 10−11). (D) Fecal albumin levels (n = 5), (E) fecal Lnc-2 content, (n = 4−5), and (F) ileal MPO activity (n = 9−14) measured in 7-day PBS- and S961-treated mice. (G, H) Flow cytometry analysis of macrophages in ileal *lamina propria* from the indicated groups of mice (n = 4−8). (I) Relative quantification of indicated cytokine mRNA levels in ileal *lamina propria* from 7-day PBS- and S961-treated mice (n = 6). (B−I) Values are means ± SEM. ns, $*p < 0.05$, $**p < 0.01$, $***p < 0.001$, $****p < 0.0001$ by ANOVA (B−C, I) or Mann−Whitney U-test (D−H).
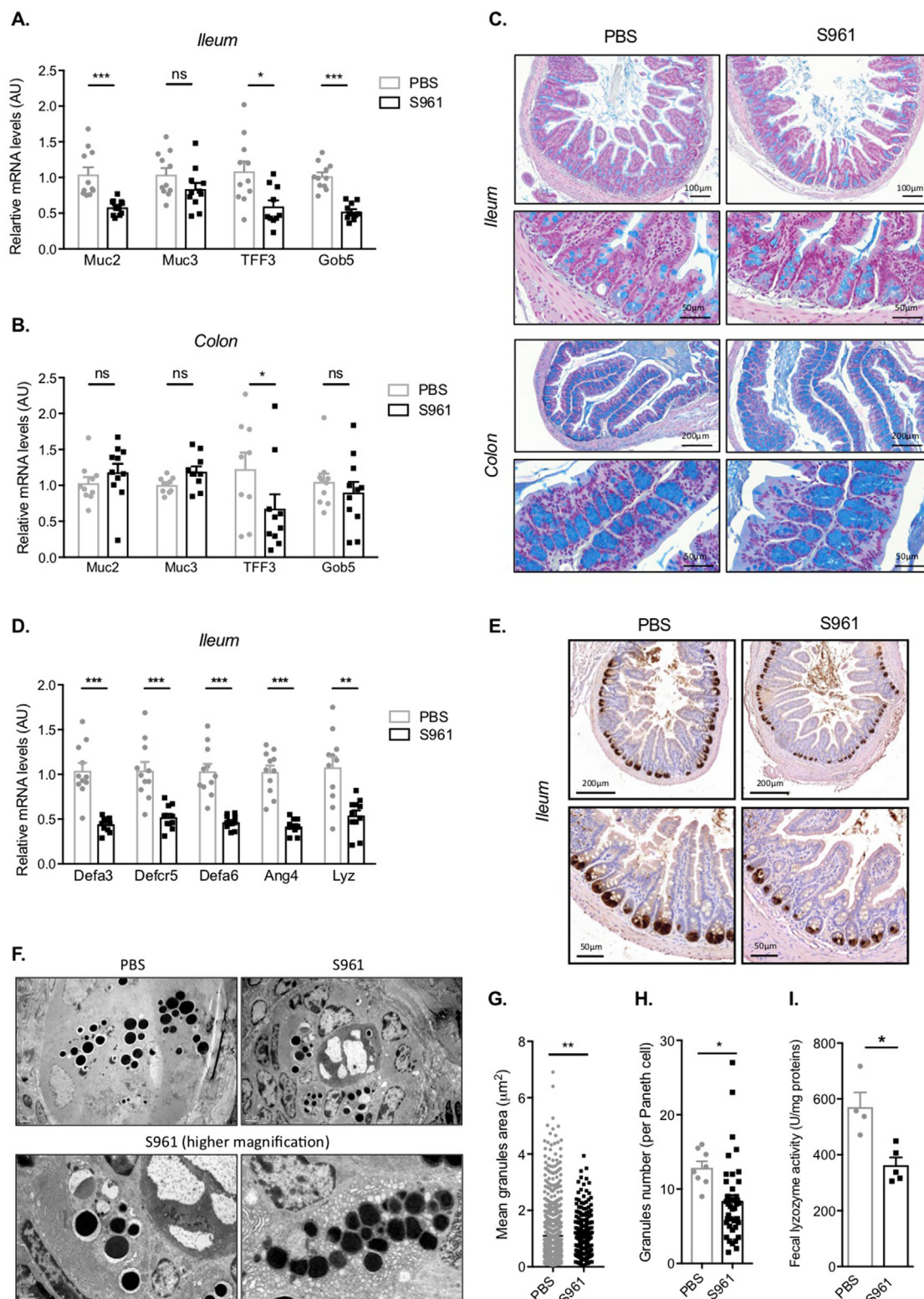
Figure 3: S961 infusion decreased antimicrobial activity of Paneth cells. (A, B) Relative mRNA levels (normalized to *Gapdh*) of goblet cell markers in ileal and colonic IECs from 7-day PBS- and S961-treated mice (n = 10−11). (C) Representative Alcian blue staining of sections from the ileum (upper panels) and the colon (lower panels) of PBS and S961 mice. (D) Relative mRNA levels (normalized to *Gapdh*) of Paneth cell markers in ileal IECs from 7-day PBS- and S961-treated mice (n = 11). (E) Representative lysozyme immunostaining of ileal sections from PBS and S961 mice. (F) Representative electron microscopy images of ileal samples from PBS- and S961-treated mice. Scale bars: 1 μm (upper panels), part 2 μm (lower panels). (G, H) Mean secretory granule area and number of Paneth cells from PBS and S961 mice after 7 days of treatment (n = 3 mice per group). Data are means from 4 to 20 arbitrary chosen electron microscopy fields per mice, with 1−6 Paneth cells per field. (I) Fecal lysozyme activity in PBS and S961 mice after 7 days of treatment (n = 4−5). (A-B, D, G-I) Values are means ± SEM. *p < 0.05, **p < 0.01, ***p < 0.001 by ANOVA (A, B, D) or Mann−Whitney U-test (G−I).

3.4. Dysbiosis associated with S961 infusion induced intestinal barrier impairment

As bactericidal activity of Paneth cells was impaired upon IR inhibition, we further investigated, through 16S rRNA gene sequencing, the potential consequences of S961 treatment on local microbiota equilibrium. Principal coordinate analysis using the Bray—Curtis distance and hierarchical clustering of luminal microbiota from the ileum of PBS- and S961-treated mice revealed that S961 treatment significantly altered the intestinal bacterial communities (Figure 4A, S5A). Three-day S961-challenged mice exhibited an intermediary profile when compared to the PBS control group and mice that received S961 for 7 days (Figure 4A, S5A). Moreover, cessation of S961 treatment allowed the rescue of an ileal microbial profile similar to PBS-infused mice (Figure 4A, S5A). A 7-day challenge with S961 triggered a reduction in ileal bacterial diversity (Figure 4B—C). While the ileal microbiota from the PBS control group was characterized, as previously described [32], by a large predominance of Firmicutes (above 90%), mice that were infused with S961 displayed an ileal bloom of pro-inflammatory Proteobacteria, in particular Enterobacteriaceae, at the expense of Bacteroidetes, Actinobacteria, and Firmicutes species (Figure 4D—E). Of note, parallel analyses of the microbiota composition in the caecum of mice receiving S961 demonstrated that S961 treatment induced similar and reversible changes in the small and large intestines, as illustrated by a 20% increase in cecal Proteobacteria abundance when compared to the 7-day PBS-challenged control group (data not shown). Interestingly, alterations of ileal and cecal microbiota composition upon 3 days of S961 treatment (Figure 4A—E, S5A) were not accompanied by major modifications in the expression of either tight junction (Fig S3B), goblet cells (Fig S4A) or Paneth cells markers (Fig S4A—B), suggesting that S961-induced dysbiosis preceded the profound epithelial defects that occurred after 7 days of insulin signal blockade (Figure 2A—B, 3A, 3D). In order to test whether microbiota imbalance could act as a triggering event in intestinal barrier disruption due to insulin resistance, 3-week-old specific-pathogen-free (SPF) C57Bl/6 J mice were transplanted with feces from PBS- (PBS FT group) or S961-treated mice (S961 FT group), and comparative analyses were further performed 7 days later. Despite similar body weight and blood glucose of recipient mice regardless of donor (Fig S6B—C), the abundance of luminal Proteobacteria and Enterobacteriaceae was enhanced in the feces of S961 FT mice when compared to the PBS FT control group (Figure 4F—G), in accordance with the gut microbiota alterations previously observed in S961-treated mice (Figure 4D—E). Of note, S961 fecal transplantation parallelly induced the onset of gut hyperpermeability, as evidenced by the relative 2-fold increase of FITC-dextran plasma concentrations in S961 FT mice respective to PBS FT mice (Figure 4H). However, the transmission of the S961-associated ileal phenotype in mice that were transplanted with the fecal microbiota from an S961 donor was only partial. Indeed, S961 fecal transplantation was not associated with changes of fecal lipocalin activity, albumin content (Figure 4I—J), or mRNA levels of Paneth cell antimicrobial peptides, goblet cell markers, and genes encoding tight junction proteins (Fig S6D—F). Altogether, these results indicated that insulin resistance and associated hyperglycemia trigger the onset of a deleterious dysbiosis, as characterized by the rise of pro-inflammatory bacterial species, which consequently contribute at least in part to gut permeability impairment.

4. DISCUSSION

The systemic low-grade inflammation that characterizes obesity and associated insulin resistance and hyperglycemia was first considered to originate from the inflamed adipose tissue. However, more recent evidence has underscored the contribution of altered gut microbiota composition and increased intestinal permeability to this feature [11,33—35]. While most of these studies have focused on the gut defects associated with obesity in mice fed with high-calorie diets, we show in S961-treated mice that, independently of adiposity, insulin resistance and concomitant hyperglycemia *per se* are key players in the rapid onset of a drastic intestinal dysbiosis as well as major epithelial dysfunctions, including impaired bactericidal defense by Paneth cells, enhanced gut permeability, and local low-grade inflammation. Moreover, we demonstrate that such imbalanced gut microbiota acts as an early initiating event of the intestinal epithelial defects upon insulin resistant states.

Gut microbial imbalance is a hallmark of various metabolic diseases, and the interaction of such dysbiotic microbiota with IEC was shown to play a pivotal role in the disruption of gut barrier integrity upon obesity [36,37]. While alterations of intestinal microbiota composition were previously also reported in lean and hyperglycemic mouse models of insulinopenia, those changes were shown not to directly affect intestinal permeability [17]. Accordingly, we demonstrate that, independently of obesity, S961-induced insulin resistance and associated hyperglycemia trigger drastic changes in both ileal and cecal microbiota composition. However, in contrast to the work by Thaiss et al., our study demonstrated that fecal transplant from S961-treated mice is sufficient to cause gut hyperpermeability, suggesting that microbiota imbalance consecutive to insulin resistance acts as one of the early triggers of intestinal barrier disruption. The protective role of proper insulin sensitivity on gut barrier integrity is also supported by the recent study by Rangan et al. [38]. Indeed, in a murine model of inflammatory bowel disease, intermittent fasting, which improves peripheral insulin sensitivity [39], was shown to alter microbiota composition by promoting the expansion of protective Lactobacillaceae and Bifidobacteriaceae, ultimately reducing systemic inflammation [38]. Furthermore, treating the mice with rosiglitazone, a PPARγ agonist that enhances insulin sensitivity in T2D patients, restored the defects induced by HFD on antimicrobial peptides expression and spatial distribution of microbiota in the ileum [40].

S961-induced ileal and cecal dysbiosis was characterized by a bloom of pro-inflammatory Proteobacteria and by a massive drop of obligate anaerobes abundance, concomitantly to the onset of a modest gut inflammation. Interestingly, obesity [41—43] and Crohn's disease [44,45] were previously associated with enrichment in fecal Proteobacteria. Among possible mechanisms underlying the onset of such a dysbiosis subsequently to defective insulin action, changes in host physiology, as observed following antibiotic treatment or infection with enteric pathogen, may increase oxygen availability and drive luminal expansion of Enterobacteriaceae [46]. While oxidative metabolism of colonocytes normally maintains epithelial hypoxia and favors a microbial community dominated by obligate anaerobic bacteria, reduced beta-oxidation capacities of IECs upon intestinal inflammation were shown to increase oxygen availability and to consequently promote dysbiosis and associated burst of Proteobacteria [47,48]. Moreover, the down-regulation of PPAR-γ signaling, as observed in diabetic insulin-deficient mice [49], was shown to increase host nitrate production, the exploitation of which by commensal Enterobacteriaceae promotes their predominance upon inflammatory conditions [50]. Altogether, these reports suggest that, in our model, insulin resistance may trigger metabolic alterations in ileal epithelial cells thereby hampering the delicate balance between the host and resident microbial communities. Nevertheless, our data indicate that the ileal blooming of Proteobacteria within 3 days of S961 treatment did not parallel major defects in various components of
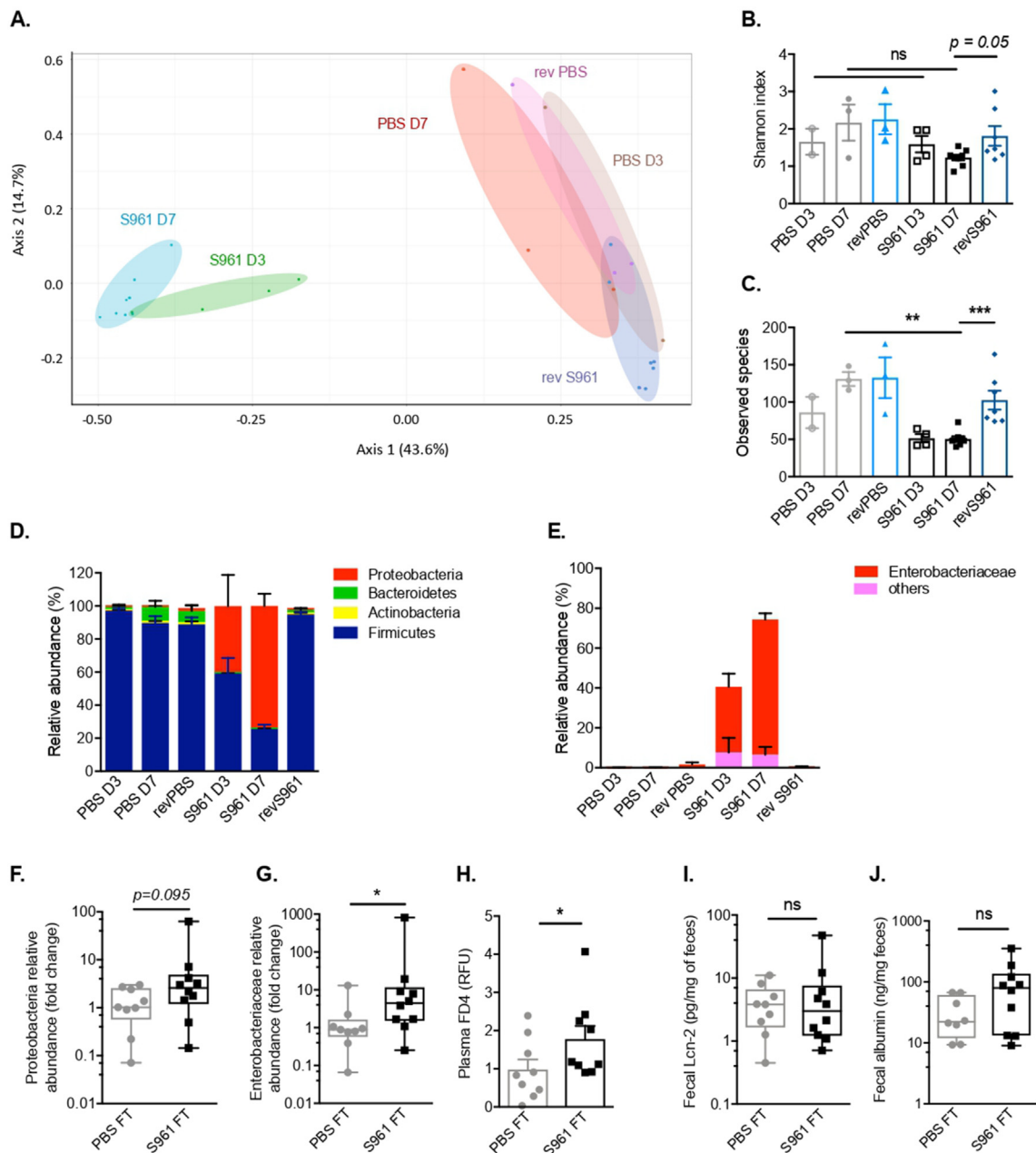
Figure 4: Dysbiosis associated with S961 treatment triggers intestinal barrier impairment. (A) Principal Coordinate Analysis (PCoA) of ileal microbiota composition in control PBS and S961 mice after 3 and 7 days of treatment, and in revPBS and revS961 mice one week after the pump removal. PCoA plots are based on Bray Curtis distance matrices (n = 2−8). (B) Shannon index and (C) number of observed species in mice treated with PBS or S961 for 3 or 7 days, or in revPBS and revS961 studied 7 days after removal of the pumps (n = 2−8). (D) Relative abundance of bacterial phyla and (E) Proteobacteria families, including Enterobacteriacae, in the ileum of mice treated with PBS or S961 for 3 (PBS D3, S961 D3) or 7 days (PBS D7, S961 D7), or studied 7 days after removal of the pumps (revPBS, revS961) (n = 2−8). Relative abundance of fecal (F) Proteobacteria and (G) Enterobacteriacae in recipient C57Bl/6 mice, 7 days after fecal transfer from PBS-or S961-treated donor mice (n = 9−10). (H) FD4 intestinal gut permeability (shown as FD4 plasma accumulation 1 h after oral gavage and normalized for transit time), (I) caecum luminal Lcn-2 levels and (J) cecum fecal albumin concentrations measured in recipient C57Bl/5 mice 7 days after fecal transfer from PBS-or S961-treated donor mice (n = 8−10). (B−J) Values are means ± SEM. ns, *p < 0.05, **p < 0.01, ***p < 0.001 by ANOVA (B, C) or Mann−Whitney U-test (F−J).

the gut barrier, indicating that dysbiosis might instead initiate epithelial dysfunctions upon insulin resistance. Further fecal transfer experiments from S961-treated mice indeed confirmed that S961-dysbiotic microbiota was sufficient to alter gut permeability. Accordingly, a direct deleterious effect of imbalanced microbiota on cell−cell junction integrity was previously demonstrated upon antibiotics treatment [51]. However, mice that were transplanted with the fecal microbiota from

S961 donor did not display any significant quantitative change in mRNA encoding tight junction proteins, suggesting that transplantation of fecal instead of ileal or cecal microbiota from S961 donor mice might not be sufficient to achieve the complete restoration of the S961-associated ileal phenotype.

Commensal microbiota is a reservoir of bacterial endotoxins that translocate into the systemic circulation upon intestinal barrier

disruption to induce metabolic endotoxemia. Under steady state conditions, intestinal epithelium forms a selective barrier allowing the transcellular transport of nutrients while rigorously excluding the paracellular flow of immune-stimulatory bacterial products across the epithelium. Tight connections between IECs through intercellular junctions actively contribute to the physical component of the gut barrier. Upon S961 treatment, global IR signaling blockade and associated hyperglycemia induced a dramatic disorganization of IECs' brush border and a breakdown of intercellular junctions in the ileum. Of note, impairment of IEC junctions was previously documented upon obese and diabetic states, in both humans [5,52,53] and animal models [14,54−56]. Moreover, recent studies demonstrated that, independently of obesity, both hyperglycemia, via a transcriptional reprogramming mediated by intestinal glucose metabolism [17], and blunted intestinal insulin signaling, via a FoxO-dependent mechanism, control the integrity of IEC intercellular junctions [57].

Among other components of the gut barrier, Paneth and goblet cells occupy a key position, as the antimicrobial peptides and the mucus they produce contribute to the host protection from enteric pathogens and bacterial translocation to the regulation of commensal microbiota composition, and local immune response. We report in this study that S961 infusion impaired intestinal bactericidal defense by Paneth cells, which likely resulted from the profound structural alterations we observed in parallel in this epithelial cell type. In accordance with this observation, a defective antimicrobial activity was previously described upon insulin-resistant state in mouse models of high-fat diet induced obesity or STZ-mediated insulinopenia [58,59]. Interestingly, ultra-structural analyses further revealed that, upon S961 treatment, Paneth cells displayed major abnormalities, including reduced number and aberrant morphology of secretory granules as well as apparent features of ER stress. Of note, reduced expression of antimicrobial peptides and activation of the unfolded protein response were reported in Paneth cells of obese patients [60]. However, molecular analyses of ileal tissue from S961-treated mice did not reveal any significant modification of the unfolded stress response, to which Paneth cells were shown to be highly sensitive in mice [31]. Our data therefore suggest either the involvement of other mechanisms downstream of IR blockade in Paneth cells disruption or underlie the need to perform further analyses on purified intestinal crypts or sorted Paneth cells.

Besides hampering bactericidal defenses, S961-associated insulin resistance affected the intestinal but not the colonic expression of goblet cell markers. Despite the fact that this was not correlated with apparent changes of epithelial mucus staining, hyperglycemia was previously associated with decreased bacterial-epithelial distance in the colon [61], supporting the contribution of impaired goblet cell secretion to barrier dysfunction upon an insulin resistant state. Accordingly, Wei et al. previously reported that a 12-day treatment with insulin in a diabetic mouse model was sufficient to restore the thickness of the colonic mucus layer and to correct associated intestinal gut hyperpermeability [18]. While the lowered expression of the fatty acid synthase (Fas), due to impaired gut insulin action, was suggested to reduce both expression and palmitoylation of the mucin Muc2 and its subsequent luminal secretion, intestinal mRNA quantification of prototypic hepatic insulin target genes encoding lipogenic enzymes (Acc, Fas, Scd1) revealed only a significant decrease of the desaturase Scd1 upon S961 challenge (data not shown). However, unchanged expression of Muc2 in mice with targeted deletion of Scd1 in the intestinal epithelium [62] suggests the involvement of other signaling pathways downstream of IR blockade in the reduced expression of goblet cell markers. Alternatively, the high vulnerability of goblet cells to ER stress that was observed in intestinal XBP1 KO mice [63] as well

as in diet-induced obesity mice model [64] might prompt further investigation in order to determine whether insulin resistance triggers ER stress in goblet cells.

Besides triggering gut dysbiosis and enhanced intestinal permeability, S961-induced insulin resistance promotes a local immune response that was illustrated by the ileal accumulation of fully mature CD11b+ CD206+ macrophages [65] and the significant increase of IL23 mRNA expression in the ileum lamina propria of S961-treated mice, consistent with previous report [25]. Accordingly, microbe-associated molecular patterns were shown to stimulate the production of IL23 by macrophages and dendritic cells upon pathogen invasion or intestinal barrier breach [66], and comprehensive analyses in human showed that IL23 mRNA levels were enhanced in combined lamina propria and epithelial fraction of jejunum from obese patients compared to lean subjects [67]. Of note, IL23 was involved in the initiation and perpetuation of both innate and T cell-mediated intestinal inflammation in various mouse models of colitis, and blockade or genetic ablation of IL23 was found to attenuate intestinal inflammation [68]. Moreover, CD11b+ macrophages, which are highly bactericidal, were shown to produce high quantities of IL-23 at the early stages of colitis and to be essential for the initiation of intestinal immunopathology [69,70]. While a higher risk of infection by enteropathogens was reported in db/db or high fat-diet fed obese and diabetic mice, in STZ-treated diabetic mice [17] as well as in diabetic patients [71], rescuing the compromised production of IL23 in obese mice after Citrobacter rodentium infection was sufficient to restore the mucosal host defense [30]. According with these observations, the blockade of insulin signaling by S961 treatment in mice were associated with enhanced susceptibility to enteric infection by C. rodentium (data not shown), suggesting that activation of the IL23-to-IL22 axis upon enteric infection might be defective during diabetes, independently of obesity.

In conclusion, this study highlights insulin signaling as an indispensable gatekeeper of gut barrier integrity and as a safeguard against local inflammation. Independent of obesity, insulin resistance and associated hyperglycemia trigger a rapid, drastic, and reversible intestinal dysbiosis, which contributes at least partly to enhanced gut permeability. Moreover, we demonstrate that insulin sensitivity is a key player in the maintenance of functional gut epithelial barrier major components, as illustrated by disrupted cell−cell adhesion, as well as the breakdown of mucus and antimicrobial peptides production upon S961 treatment. Altogether, our data suggest that, besides enhanced adiposity, the detrimental consequences of global insulin resistance on the gut epithelium and associated microbiota might contribute to the onset of chronic low-grade systemic inflammation and the increased risk of acute enteric infections during metabolic syndrome.

AUTHORS' CONTRIBUTION

ACKNOWLEDGEMENTS

CONFLICT OF INTEREST

The authors declare that they have no known competing financial interests or personal relationships that could have appeared to influence the work reported in this paper.

APPENDIX A. SUPPLEMENTARY DATA

Supplementary data to this article can be found online at https://doi.org/10.1016/j.molmet.2022.101438.

REFERENCES

[1] Gregor, M.F., Hotamisligil, G.S., 2011. Inflammatory mechanisms in obesity. Annual Review of Immunology 29:415—445.

[2] Wellen, K.E., Hotamisligil, G.S., 2005. Inflammation, stress, and diabetes. Journal of Clinical Investigation 115:1111—1119.

[3] Teixeira, T.F., Collado, M.C., Ferreira, C.L., Bressan, J., Peluzio Mdo, C., 2012. Potential mechanisms for the emerging link between obesity and increased intestinal permeability. Nutrition Research 32:637—647.

[4] Verdam, F.J., Fuentes, S., de Jonge, C., Zoetendal, E.G., Erbil, R., Greve, J.W., et al., 2013. Human intestinal microbiota composition is associated with local and systemic inflammation in obesity. Obesity 21:E607—E615.

[5] Genser, L., Aguanno, D., Soula, H.A., Dong, L., Trystram, L., Assmann, K., et al., 2018. Increased jejunal permeability in human obesity is revealed by a lipid challenge and is linked to inflammation and type 2 diabetes. The Journal of Pathology 246:217—230.

[6] Dalmas, E., Rouault, C., Abdennour, M., Rovere, C., Rizkalla, S., Bar-Hen, A., et al., 2011. Variations in circulating inflammatory factors are related to changes in calorie and carbohydrate intakes early in the course of surgery-induced weight reduction. The American Journal of Clinical Nutrition 94:450—458.

[7] Calder, P.C., Ahluwalia, N., Brouns, F., Buetler, T., Clement, K., Cunningham, K., et al., 2011. Dietary factors and low-grade inflammation in relation to overweight and obesity. British Journal of Nutrition 106(Suppl 3):S5—S78.

[8] Grant, R.W., Dixit, V.D., 2015. Adipose tissue as an immunological organ. Obesity 23:512—518.

[9] Cox, A.J., West, N.P., Cripps, A.W., 2015. Obesity, inflammation, and the gut microbiota. Lancet Diabetes & Endocrinology 3:207—215.

[10] Peterson, L.W., Artis, D., 2014. Intestinal epithelial cells: regulators of barrier function and immune homeostasis. Nature Reviews Immunology 14:141—153.

[11] Cani, P.D., Amar, J., Iglesias, M.A., Poggi, M., Knauf, C., Bastelica, D., et al., 2007. Metabolic endotoxemia initiates obesity and insulin resistance. Diabetes 56:1761—1772.

[12] Clemente-Postigo, M., Oliva-Olivera, W., Coin-Araguez, L., Ramos-Molina, B., Giraldez-Perez, R.M., Lhamyani, S., et al., 2019. Metabolic endotoxemia promotes adipose dysfunction and inflammation in human obesity. American Journal of Physiology. Endocrinology and Metabolism 316:E319—E332.

[13] Miele, L., Valenza, V., La Torre, G., Montalto, M., Cammarota, G., Ricci, R., et al., 2009. Increased intestinal permeability and tight junction alterations in nonalcoholic fatty liver disease. Hepatology 49:1877—1887.

[14] Cani, P.D., Bibiloni, R., Knauf, C., Waget, A., Neyrinck, A.M., Delzenne, N.M., et al., 2008. Changes in gut microbiota control metabolic endotoxemia-induced inflammation in high-fat diet-induced obesity and diabetes in mice. Diabetes 57:1470—1481.

[15] Araujo, J.R., Tomas, J., Brenner, C., Sansonetti, P.J., 2017. Impact of high-fat diet on the intestinal microbiota and small intestinal physiology before and after the onset of obesity. Biochimie 141:97—106.

[16] Winer, D.A., Luck, H., Tsai, S., Winer, S., 2016. The intestinal immune system in obesity and insulin resistance. Cell Metabolism 23:413—426.

[17] Thaiss, C.A., Levy, M., Grosheva, I., Zheng, D., Soffer, E., Blacher, E., et al., 2018. Hyperglycemia drives intestinal barrier dysfunction and risk for enteric infection. Science 359:1376—1383.

[18] Wei, X., Yang, Z., Rey, F.E., Ridaura, V.K., Davidson, N.O., Gordon, J.I., et al., 2012. Fatty acid synthase modulates intestinal barrier function through palmitoylation of mucin 2. Cell Host & Microbe 11:140—152.

[19] Yu, S., Tong, K., Zhao, Y., Balasubramanian, I., Yap, G.S., Ferraris, R.P., et al., 2018. Paneth cell multipotency induced by notch activation following injury. Cell Stem Cell 23:46—59 e45.

[20] Hosokawa, M., Dolci, W., Thorens, B., 2001. Differential sensitivity of GLUT1- and GLUT2-expressing beta cells to streptozotocin. Biochemical and Biophysical Research Communications 289:1114—1117.

[21] Miyamoto, K., Hase, K., Taketani, Y., Minami, H., Oka, T., Nakabou, Y., et al., 1991. Diabetes and glucose transporter gene expression in rat small intestine. Biochemical and Biophysical Research Communications 181:1110—1117.

[22] Leturque, A., Brot-Laroche, E., Le Gall, M., 2009. GLUT2 mutations, translocation, and receptor function in diet sugar managing. American Journal of Physiology. Endocrinology and Metabolism 296:E985—E992.

[23] Lengeler, J., 1980. Analysis of the physiological effects of the antibiotic streptozotocin on Escherichia coli K 12 and other sensitive bacteria. Archives of Microbiology 128:196—203.

[24] Gusarova, V., Alexa, C.A., Na, E., Stevis, P.E., Xin, Y., Bonner-Weir, S., et al., 2014. ANGPTL8/betatrophin does not control pancreatic beta cell expansion. Cell 159:691—696.

[25] Rouland, M., Beaudoin, L., Rouxel, O., Bertrand, L., Cagninacci, L., Saffarian, A., et al., 2022. Gut mucosa alterations and loss of segmented filamentous bacteria in type 1 diabetes are associated with inflammation rather than hyperglycaemia. Gut 71:296—308.

[26] Escudie, F., Auer, L., Bernard, M., Mariadassou, M., Cauquil, L., Vidal, K., et al., 2018. FROGS: find, rapidly, OTUs with galaxy solution. Bioinformatics 34:1287—1294.

[27] Le Roy, T., Debedat, J., Marquet, F., Da-Cunha, C., Ichou, F., Guerre-Millo, M., et al., 2018. Comparative evaluation of microbiota engraftment following fecal microbiota transfer in mice models: age, kinetic and microbial status matter. Frontiers in Microbiology 9:3289.

[28] Michael, M.D., Kulkarni, R.N., Postic, C., Previs, S.F., Shulman, G.I., Magnuson, M.A., et al., 2000. Loss of insulin signaling in hepatocytes leads to severe insulin resistance and progressive hepatic dysfunction. Molecular Cell 6:87—97.

[29] Otani, T., Furuse, M., 2020. Tight junction structure and function revisited. Trends in Cell Biology 30:805—817.

[30] Wang, X., Ota, N., Manzanillo, P., Kates, L., Zavala-Solorio, J., Eidenschenk, C., et al., 2014. Interleukin-22 alleviates metabolic disorders and restores mucosal immunity in diabetes. Nature 514:237—241.

[31] Clevers, H.C., Bevins, C.L., 2013. Paneth cells: maestros of the small intestinal crypts. Annual Review of Physiology 75:289—311.

[32] Jakobsson, H.E., Rodríguez-Piñeiro, A.M., Schütte, A., Ermund, A., Boysen, P., Bemark, M., et al., 2015. The composition of the gut microbiota shapes the colon mucus barrier. EMBO Reports 16:164—177.

[33] Ding, S., Chi, M.M., Scull, B.P., Rigby, R., Schwerbrock, N.M., Magness, S., et al., 2010. High-fat diet: bacteria interactions promote intestinal inflammation which precedes and correlates with obesity and insulin resistance in mouse. PLoS One 5:e12191.

Original Article

[34] Liu, Z., Brooks, R.S., Ciappio, E.D., Kim, S.J., Crott, J.W., Bennett, G., et al., 2012. Diet-induced obesity elevates colonic TNF-alpha in mice and is accompanied by an activation of Wnt signaling: a mechanism for obesity-associated colorectal cancer. The Journal of Nutritional Biochemistry 23:1207—1213.

[35] Winer, S., Paltser, G., Chan, Y., Tsui, H., Engleman, E., Winer, D., et al., 2009. Obesity predisposes to Th17 bias. European Journal of Immunology 39:2629—2635.

[36] Cani, P.D., Osto, M., Geurts, L., Everard, A., 2012. Involvement of gut microbiota in the development of low-grade inflammation and type 2 diabetes associated with obesity. Gut Microbes 3:279—288.

[37] Qin, J., Li, Y., Cai, Z., Li, S., Zhu, J., Zhang, F., et al., 2012. A metagenome-wide association study of gut microbiota in type 2 diabetes. Nature 490:55—60.

[38] Rangan, P., Choi, I., Wei, M., Navarrete, G., Guen, E., Brandhorst, S., et al., 2019. Fasting-mimicking diet modulates microbiota and promotes intestinal regeneration to reduce inflammatory bowel disease pathology. Cell Reports 26: 2704—2719 e2706.

[39] Fabbiano, S., Suarez-Zamorano, N., Chevalier, C., Lazarevic, V., Kieser, S., Rigo, D., et al., 2018. Functional gut microbiota remodeling contributes to the caloric restriction-induced metabolic improvements. Cell Metabolism 28:907—921 e907.

[40] Tomas, J., Mulet, C., Saffarian, A., Cavin, J.B., Ducroc, R., Regnault, B., et al., 2016. High-fat diet modifies the PPAR-gamma pathway leading to disruption of microbial and physiological ecosystem in murine small intestine. Proceedings of the National Academy of Sciences of the United States of America 113:E5934—E5943.

[41] Turnbaugh, P.J., Ley, R.E., Mahowald, M.A., Magrini, V., Mardis, E.R., Gordon, J.I., 2006. An obesity-associated gut microbiome with increased capacity for energy harvest. Nature 444:1027—1031.

[42] Lambeth, S.M., Carson, T., Lowe, J., Ramaraj, T., Leff, J.W., Luo, L., et al., 2015. Composition, diversity and abundance of gut microbiome in prediabetes and type 2 diabetes. Journal of Diabetes, Obesity & Metabolism 2:1—7.

[43] Fei, N., Zhao, L., 2013. An opportunistic pathogen isolated from the gut of an obese human causes obesity in germfree mice. The ISME Journal 7:880—884.

[44] Garrett, W.S., Gallini, C.A., Yatsunenko, T., Michaud, M., DuBois, A., Delaney, M.L., et al., 2010. Enterobacteriaceae act in concert with the gut microbiota to induce spontaneous and maternally transmitted colitis. Cell Host & Microbe 8:292—300.

[45] Huttenhower, C., Kostic, A.D., Xavier, R.J., 2014. Inflammatory bowel disease as a model for translating the microbiome. Immunity 40:843—854.

[46] Rivera-Chavez, F., Lopez, C.A., Baumler, A.J., 2017. Oxygen as a driver of gut dysbiosis. Free Radical Biology and Medicine 105:93—101.

[47] Hughes, E.R., Winter, M.G., Duerkop, B.A., Spiga, L., Furtado de Carvalho, T., Zhu, W., et al., 2017. Microbial respiration and formate oxidation as metabolic signatures of inflammation-associated dysbiosis. Cell Host & Microbe 21: 208—219.

[48] Litvak, Y., Byndloss, M.X., Baumler, A.J., 2018. Colonocyte metabolism shapes the gut microbiota. Science 362.

[49] Vidal-Puig, A., Jimenez-Linan, M., Lowell, B.B., Hamann, A., Hu, E., Spiegelman, B., et al., 1996. Regulation of PPAR gamma gene expression by nutrition and obesity in rodents. Journal of Clinical Investigation 97:2553—2561.

[50] Winter, S.E., Winter, M.G., Xavier, M.N., Thiennimitr, P., Poon, V., Keestra, A.M., et al., 2013. Host-derived nitrate boosts growth of E. coli in the inflamed gut. Science 339:708—711.

[51] Feng, Y., Huang, Y., Wang, Y., Wang, P., Song, H., Wang, F., 2019. Antibiotics induced intestinal tight junction barrier dysfunction is associated with microbiota dysbiosis, activated NLRP3 inflammasome and autophagy. PLoS One 14: e0218384.

[52] Marchiando, A.M., Graham, W.V., Turner, J.R., 2010. Epithelial barriers in homeostasis and disease. Annual Review of Pathology: Mechanisms of Disease 5:119—144.

[53] Kojima, T., Fuchimoto, J., Yamaguchi, H., Ito, T., Takasawa, A., Ninomiya, T., et al., 2010. c-Jun N-terminal kinase is largely involved in the regulation of tricellular tight junctions via tricellulin in human pancreatic duct epithelial cells. Journal of Cellular Physiology 225:720—733.

[54] Johnson, A.M., Costanzo, A., Gareau, M.G., Armando, A.M., Quehenberger, O., Jameson, J.M., et al., 2015. High fat diet causes depletion of intestinal eosinophils associated with intestinal permeability. PLoS One 10:e0122195.

[55] Hamilton, M.K., Boudry, G., Lemay, D.G., Raybould, H.E., 2015. Changes in intestinal barrier function and gut microbiota in high-fat diet-fed rats are dynamic and region dependent. American Journal of Physiology - Gastrointestinal and Liver Physiology 308:G840—G851.

[56] Murakami, Y., Tanabe, S., Suzuki, T., 2016. High-fat diet-induced intestinal hyperpermeability is associated with increased bile acids in the large intestine of mice. Journal of Food Science 81:H216—H222.

[57] Ostermann, A.L., Wunderlich, C.M., Schneiders, L., Vogt, M.C., Woeste, M.A., Belgardt, B.F., et al., 2018. Intestinal insulin/IGF1 signaling through FoxO1 regulates epithelial integrity and susceptibility to colon cancer. Nature Metabolism 1:371—389.

[58] Yu, T., Yang, H.S., Lu, X.J., Xia, Z.S., Ouyang, H., Shan, T.D., et al., 2016. Association of bactericidal dysfunction of Paneth cells in streptozotocin-induced diabetic mice with insulin deficiency. Medical Science Monitor 22:3062—3072.

[59] Lee, J.C., Lee, H.Y., Kim, T.K., Kim, M.S., Park, Y.M., Kim, J., et al., 2017. Obesogenic diet-induced gut barrier dysfunction and pathobiont expansion aggravate experimental colitis. PLoS One 12:e0187515.

[60] Hodin, C.M., Verdam, F.J., Grootjans, J., Rensen, S.S., Verheyen, F.K., Dejong, C.H., et al., 2011. Reduced Paneth cell antimicrobial protein levels correlate with activation of the unfolded protein response in the gut of obese individuals. The Journal of Pathology 225:276—284.

[61] Chassaing, B., Raja, S.M., Lewis, J.D., Srinivasan, S., Gewirtz, A.T., 2017. Colonic microbiota encroachment correlates with dysglycemia in humans. Cellular and Molecular Gastroenterology and Hepatology 4:205—221.

[62] Ducheix, S., Peres, C., Hardfeldt, J., Frau, C., Mocciaro, G., Piccinin, E., et al., 2018. Deletion of stearoyl-CoA desaturase-1 from the intestinal epithelium promotes inflammation and tumorigenesis, reversed by dietary oleate. Gastroenterology 155:1524—1538 e1529.

[63] Kaser, A., Lee, A.H., Franke, A., Glickman, J.N., Zeissig, S., Tilg, H., et al., 2008. XBP1 links ER stress to intestinal inflammation and confers genetic risk for human inflammatory bowel disease. Cell 134:743—756.

[64] Zhou, H., Zhou, S.Y., Gillilland III, M., Li, J.Y., Lee, A.H., Gao, J., et al., 2020. Bile acid toxicity in Paneth cells contributes to gut dysbiosis induced by high-fat feeding. Journal of Clinical Investigation Insight 5:e138881.

[65] Joeris, T., Muller-Luda, K., Agace, W.W., Mowat, A.M., 2017. Diversity and functions of intestinal mononuclear phagocytes. Mucosal Immunology 10:845—864.

[66] Maynard, C.L., Elson, C.O., Hatton, R.D., Weaver, C.T., 2012. Reciprocal interactions of the intestinal microbiota and immune system. Nature 489:231—241.

[67] Monteiro-Sepulveda, M., Touch, S., Mendes-Sa, C., Andre, S., Poitou, C., Allatif, O., et al., 2015. Jejunal T cell inflammation in human obesity correlates with decreased enterocyte insulin signaling. Cell Metabolism 22:113—124.

[68] Hue, S., Ahern, P., Buonocore, S., Kullberg, M.C., Cua, D.J., McKenzie, B.S., et al., 2006. Interleukin-23 drives innate and T cell-mediated intestinal inflammation. Journal of Experimental Medicine 203:2473—2483.

[69] Arnold, I.C., Mathisen, S., Schulthess, J., Danne, C., Hegazy, A.N., Powrie, F., 2016. CD11c(+) monocyte/macrophages promote chronic Helicobacter hepaticus-induced intestinal inflammation through the production of IL-23. Mucosal Immunology 9:352—363.

[70] Zigmond, E., Varol, C., Farache, J., Elmaliah, E., Satpathy, A.T., Friedlander, G., et al., 2012. Ly6C hi monocytes in the inflamed colon give rise to proinflammatory effector cells and migratory antigen-presenting cells. Immunity 37:1076—1090.

[71] Yao, M.J., Li, J.Y., Li, J.Z., Wu, T.F., Xu, J.H., Huang, C.Z., et al., 2018. Diabtetes mellitus increases the risk of enteric infection: a meta-analysis. International Journal of Clinical and Experimental Medicine 11:5457—5468.